

Article

Synthesis and Characterization of Pd-Ni Bimetallic Nanoparticles as Efficient Adsorbent for the Removal of Acid Orange 8 Present in Wastewater

Ali Umar¹, Muhammad Sufaid Khan¹ , Sultan Alam¹, Ivar Zekker^{2,*}, Juris Burlakovs³, Steven S. dC Rubin^{4,5} , Gourav Dhar Bhowmick⁶, Anna Kallistova⁷, Nikolai Pimenov⁷ and Muhammad Zahoor^{8,*} 

- ¹ Department of Chemistry, University of Malakand, Chakdara Dir Lower, Khyber Pakhtunkhwa 18800, Pakistan; aliumar3937@gmail.com (A.U.); sufaidkhan1984@gmail.com (M.S.K.); dr.sultanalam@yahoo.com (S.A.)
 - ² Institute of Chemistry, University of Tartu, 14a Ravila St., 50411 Tartu, Estonia
 - ³ Institute of Forestry and Rural Engineering, Estonian University of Life Sciences, 5 Kreutzwaldi St., 51014 Tartu, Estonia; Juris.burlakovs@emu.ee
 - ⁴ Georges Lamaitre Center for Earth and Climate Research, Earth and Life Institute, Université Catholique de Louvain, B-1348 Gante, Belgium; sergio.rubin@uclouvain.be
 - ⁵ Centro Nacional de Investigaciones Biotecnológicas, CNIB, 429 Cala Cala, Cochabamba, Bolivia
 - ⁶ Department of Agricultural and Food Engineering, Indian Institute of Technology Kharagpur, Kharagpur 721302, India; gourav.db@gmail.com
 - ⁷ Research Centre of Biotechnology of the Russian Academy of Sciences, Winogradsky Institute of Microbiology, Leninsky Prospect, 33, build. 2, 119071 Moscow, Russia; kallistoanna@mail.ru (A.K.); npimenov@mail.ru (N.P.)
 - ⁸ Department of Biochemistry, University of Malakand, Chakdara Dir Lower, Khyber Pakhtunkhwa 18800, Pakistan
- * Correspondence: ivar.zekker@ut.ee (I.Z.); mohammadzahoorus@yahoo.com (M.Z.)



Citation: Umar, A.; Khan, M.S.; Alam, S.; Zekker, I.; Burlakovs, J.; dC Rubin, S.S.; Bhowmick, G.D.; Kallistova, A.; Pimenov, N.; Zahoor, M. Synthesis and Characterization of Pd-Ni Bimetallic Nanoparticles as Efficient Adsorbent for the Removal of Acid Orange 8 Present in Wastewater. *Water* **2021**, *13*, 1095. <https://doi.org/10.3390/w13081095>

Academic Editor: Laura Bulgariu

Received: 10 March 2021

Accepted: 10 April 2021

Published: 15 April 2021

Publisher's Note: MDPI stays neutral with regard to jurisdictional claims in published maps and institutional affiliations.



Copyright: © 2021 by the authors. Licensee MDPI, Basel, Switzerland. This article is an open access article distributed under the terms and conditions of the Creative Commons Attribution (CC BY) license (<https://creativecommons.org/licenses/by/4.0/>).

Abstract: In this study palladium-nickel (Pd-Ni) nanoparticles supported on carbon and cerium oxide (Pd-Ni/AC-CeO₂) were synthesized by a transfer phase method and characterized by scanning electronic microscopy (SEM), X-ray diffraction (XRD), and energy-dispersive X-ray spectroscopy (EDX). The XRD and SEM data concluded the presence of alloy formation between Pd and Ni. The synthesized particles were used as an adsorbent for removal of azo dye acid orange-8 (AO-8) from water and were found to be effective in removal (over 90% removal efficiency) of the selected dye. Different kinetics and equilibrium models were applied to calculate the adsorption parameters. The most suitable model that best fitted the equilibrium data was the Langmuir model and maximum adsorption capacities were 666.6, 714 and 769 mg/g at 293, 313 and 333 K, respectively, with R² values closed to 1 while in the case of the kinetics data the best fit was obtained with a pseudo-second order kinetics model with a high R² value. Furthermore, the adsorption thermodynamics parameters such as free energy, enthalpy, and entropy were calculated and the adsorption process was found to be exothermic with a value of ΔH° (−7.593 kJ mol^{−1}), spontaneous as ΔG° values were negative (−18.7327, −19.4870, and −20.584 kJ/mol at 293, 313 and 333 K, respectively). A positive entropy change ΔS° with a value of 0.0384 kJ /mol K indicates increased disorder at the solid–solution interface during the adsorption process. An attempt was made to recycle the Pd-Ni/AC-CeO₂ with suitable solvents and the recycled adsorbent was reused for 6 cycles with AO-8 removal efficiency up to 80%. Based on findings of the study, the synthesized adsorbent could effectively be used for the removal of other pollutants from wastewater, however, further studies are needed to prove the mechanisms.

Keywords: nanoparticles; synthesized; transfer phase method; temperatures; solutions

1. Introduction

Various industries i.e., plastic, leather, textiles, etc. use different synthetic dyes (azo dyes) to color surfaces of material objects and protect them from corrosive and environmental damage. Acid orange-8 (AO-8) is one of the most hazardous azo dyes that is used to color polyamide and wool fibers. Degradation and decolorization of textile dyes by different microbial strains have been shown in a recent study [1]. Low contents (4.5–15 mg/L) of AO-7, AO-8 and other azo dyes have been shown to be represented in water and there are possibilities of treatment with aerobic decolorization techniques. The World Health Organization has estimated the share of dyes from textiles industry in water pollution that is about 17% to 20% of all the industrial water pollution sources. In the textile industry about 80% of the dyes used are azo dyes out of which nearly 10% to 15% are discharged into wastewater treatment plant effluent and enter water bodies thereby causing water pollution. Discharge of azo dyes alter pH and chemical composition of water and thus, cause environmental imbalance, and an increase in chemical oxygen demand (COD) and biological oxygen demand (BOD) of water. Along with interferences in light penetrations, dyes' presence leads to acute toxicity of the aquatic environment. Metanil yellow, an azo dye, has exhibited hepatotoxic effects in albino rats. The azo dyes are non-biodegradable and, overall, they are carcinogenic in nature due to the presence of the $-N=N-$ (azo-) chemical bond [1–4].

Nanoparticles (NPs) are applied in various fields [5], such as in water treatment due to NPs' characteristic magnetic [6], mechanical [7], optical [8], and electrical [9] properties. NPs have been prepared by different mechanisms including incipient wetness impregnation [10], hydrothermal mechanisms [11], precipitation [12], co-precipitation [13], sputtering [14] and vapor phase mechanisms [15] etc. NPs are widely used in medicine production [16], cosmetics [17], textiles [18], leather [19], the petroleum industry [20], and catalysis [21]. Moreover, they are also used for the degradation or removal of toxic dyes, pesticides, drugs, and heavy metals present in wastewater [22–26].

The dye-containing wastewater has toxicity to the water ecosystem, reducing the transmittance of light into water depths leading to a gradual disruption and destruction of the aquatic ecosystem [27]. The degradation products of these dyes eventually reach humans thereby affecting public health. In some cases, degradation products of these dyes are carcinogenic, mutagenic and allergenic [28]. In order to preserve the aquatic environment as well as human health, the wastewater must be treated properly to minimize dye residues in it. Methods used for wastewater treatment are: flocculation, coagulation, membrane extraction, chemical precipitation, solvent extraction, ion exchange, oxidation and adsorption [29]. Among these techniques, adsorption is the most effective because of its low cost, simplicity, availability of a variety of raw materials and high efficiencies of the adsorbents. A number of adsorbents like activated sludge, rice husk ash, activated alumina, fuller's earth, fly ash, sawdust, neem bark [30] and activated carbon [31] have been used for removal of dyes from water, including azo dye (AO-8). Among them, activated carbon is widely applied as an adsorbent due to its vast surface area and prerequisite adsorption capacities. The dye removal efficiencies of activated carbon could be further enhanced if it is impregnated with various metals and metal alloys like NiO_2 , Au, Fe, Ag, Cu, etc. [32–36].

In the present study, bimetallic Pd-Ni nanoparticles were synthesized and loaded on activated carbon as well as on cerium oxide (CeO_2). The removal of AO-8 as azo dye from wastewater were studied with different isotherm and kinetics models.

2. Materials and Methods

2.1. Chemicals and Instruments Used

Chemicals applied in tests were of characteristic analytical grade, manufactured by Sigma Aldrich and in tests used without any additional purification. Acid orange 8 (AO-8) dye was purchased from Sigma Aldrich (Figure 1). The physicochemical properties of the selected dye are given in Table 1. Other chemicals used in this study were: palladium (II) chloride ($PdCl_2$ >9%), nickel (II) chloride hexahydrate ($NiCl_2 \cdot 6H_2O$, >99%), activated

carbon (AC), tetraethyl ammonium bromide (TOABr, >99%), sodium borohydride (NaBH_4), oleic acid, oleylamine, sodium hydroxide (NaOH , >99%), potassium hydroxide (KOH , >99%), sulphuric acid (H_2SO_4 , >99%), toluene, ethanol, acetone, chloroform, 2-propanol and n-hexane.

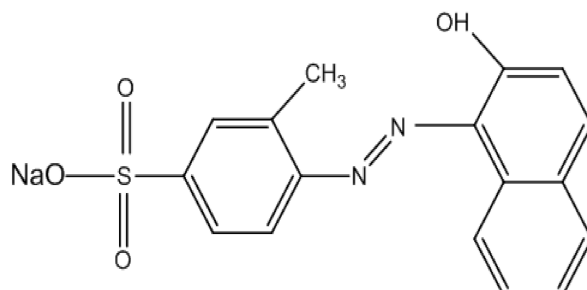


Figure 1. Structure of acid orange 8 (AO-8).

Table 1. Physiochemical properties of acid orange 8.

Name of Dye	Acid Orange 8
Molecular Formula	$\text{C}_{17}\text{H}_{13}\text{N}_2\text{NaO}_4\text{S}$
Molecular Weight	364.4 g/mol
λ_{max}	490 nm
Dye content	65 %
Water solubility	Soluble in water 1 mg/mL
Solubility in other solvents	Acetone and ethanol, insoluble in other organic solvents
Refractive Index	$n_{\text{D}}^{20} \sim 1.66$
Complexity	566
Manufacturing method	4-Amino 3 methylebenzenesulfonic acid dia azo and Naphtalen-2-ol Coupling
Usage	wool, silk, cotton, vinegar, polyamide fiber, paper, leather dyeing

2.2. Instrumentation

The samples were characterized by scanning electron microscopy (SEM) (JSM5910, JEOL, Tokyo, Japan) with SEM and energy-dispersive X-ray spectroscopy (EDX) detectors (INCA200/Oxford Instruments, Oxfordshire, UK), X-ray Diffractometer (JDX 3532, JEOL, Japan) with $\text{CuK}\alpha$ source, in Centralized Resource Laboratory at University of Peshawar, Pakistan. The dye concentration was determined by measuring absorbance using a double beam ultraviolet–visible (UV–vis) spectrophotometer (UV-1800, Shimadzu Scientific Instruments Inc., Kyoto, Japan) at a wavelength of 490 nm. Adsorption experiments were conducted in a thermostatic water-bath shaker. The pH measurements were carried out using pH meter.

2.3. Synthesis of Pd-Ni Nanoparticles Supported on Activated Carbon and Cerium Oxide

Pd-Ni nanoparticles were prepared (Figure 2) by the transfer phase method applying a slight modification (the addition of capping agents like oleic acid and oleylamine). Specifically, in the method, 5.60 mL of water solution of PdCl_2 (0.022 M) and 5.6 mL water solution of NiCl_2 (0.033 M) were supplemented to a solution of phase-transfer chemical (namely, tetraoctyl ammonium bromide—ToABr) in toluene (0.538 g of TOABr added into 37 mL of pure toluene). The solution was mixed during 2 h. The aqueous phase was separated from the toluene phase and discarded. Furthermore, the capping substrates (23.4 μL of oleic acid and 46 μL of oleylamine) were supplemented and mixed for 30 min. To make reductions of the Pd^{2+} to Pd^0 and Ni^{2+} to Ni^0 , 35 mL of NaBH_4 (0.2 M) solution was drop- wisely injected and the solution was mixed during 12 h. Thereafter, the toluene phase consisted of Pd-Ni colloidal particles, phase transferring agent (ToABr) and residues of the reducer, which were then washed with solution of dilute solution of KOH (5 mM) and distilled water. To deposit Pd-Ni particles on support, 60 mg activated carbon and 20 mg

cerium oxide were added. After addition, the mixture was stirred for 12 h. The resulting powder of Pd-Ni impregnated on activated carbon (Pd-Ni/AC-CeO₂) were filtered. To remove traces of TOABr, reducer and capping agents, which might have remained in the toluene phase, the system was washed with ethanol, acetone, toluene, and chloroform. After water addition and washing, the powder was filtered and was dispensed into a dilute solution containing KOH in ethanol and the solution was homogenized in ultrasonic treatment for 80 min. After sonication the powders were filtered and washed with ethanol, acetone and ultrapure water thoroughly. The manufactured powder was stored in an oven at 80 °C for 2 h and then stored in bottles until further use.

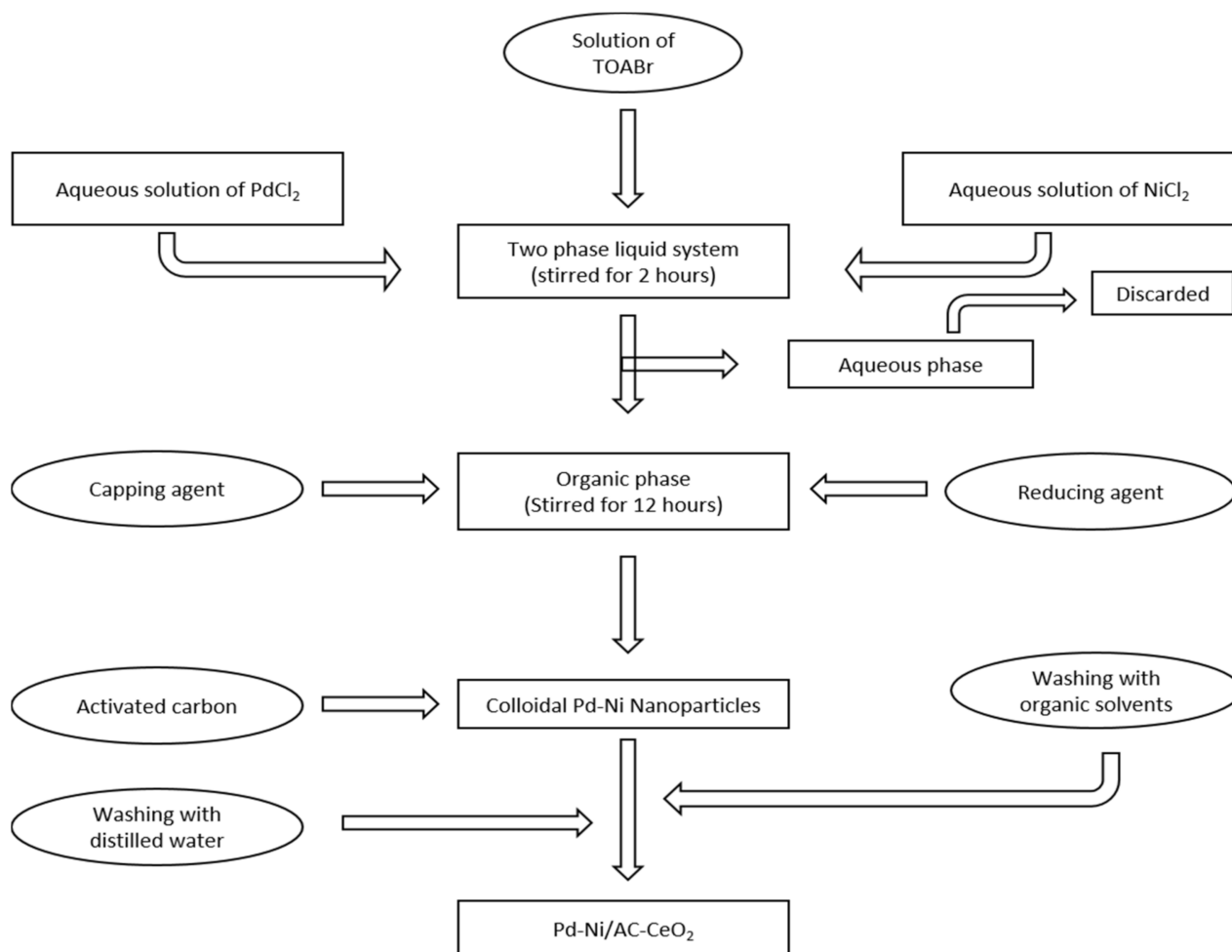


Figure 2. Preparation of Pd-Ni bimetallic nanoparticles.

2.4. Adsorption Experiments

The adsorption performance of acid orange 8 (AO-8) dye in water medium was measured in a fed-batch tests at pH 2. In tests, 0.01 g Pd-Ni/AC-CeO₂ were stirred using 10 mL solution of dye (AO-8). pH of the solution was fixed by supplementing small amounts of acidic chemical of HCl (1 M). Thereafter, the solutions were mixed in a thermostatic water-bath shaker for specific time till homogenization occurred. At predetermined time, reagent bottles were withdrawn from the shaker, the adsorbent was filtered and dye concentration in filtrate was determined by UV-vis spectrophotometer at $\lambda_{\max} = 490$ nm. The dye contents were measured according to calibration measurements

at different wavelengths over concentration measures. The capacity of adsorption on adsorbent q_t (mg/g) and dye removal efficiency were calculated by the following equations:

$$q_t = \frac{C_0 - C_t}{W} V \quad (1)$$

$$\%R = \frac{C_0 - C_t}{C_0} \times 100 \quad (2)$$

where, q_t is the amount of dye adsorbed (mg/g), %R is dye removal efficiency, C_0 is initial dye concentration (mg/L), C_t is dye concentration after adsorption, V is volume of dye solution (mL), W is the weight of adsorbent (g).

Equilibrium adsorption experiments were performed on different mixtures in the range 50–500 mg/L with prepared adsorbent of 0.01 g. The pH of these samples was adjusted to 2 and subsequently after supplementing the adsorbent solutions were mixed for 1 h. The separation of adsorbent was thereafter done from the mixture by filtration and residual contents were measured by UV–vis spectrometer.

Studies on kinetics were done with 100 mg/L solutions while remaining parameters were same as described above. Similarly, effects of adsorbent dosage, pH (2–12) and temperature were determined for 100 mg/L solutions sustaining the rest of the measures unchanged.

3. Results and Discussion

3.1. Characterization

3.1.1. Scanning Electron Microscopy (SEM)

The morphological studies of Pd-Ni nanoparticles supported on activated carbon and cerium oxide were carried out using SEM analysis. The SEM images are shown in Figure 3a–d. The micrographs show rough interfaces along with many cavities while nanoparticles are randomly spread on the surface. Surface morphology showed characteristic irregular channels of nanoparticles that could be used as an adsorption mechanism of the dye.

3.1.2. X-Ray Diffraction (XRD) and Energy-Dispersive X-Ray (EDX) Measures of Pd-Ni/AC-CeO₂ Nanoparticles

The crystallite size was computed from the Scherer formula, being at 6 (± 2) nm, while the crystallinity was found to be 75%. The characteristic peaks of cerium oxide were observed at 2θ values of 28.5, 33.08, 47.48, 56.3, 59.087, 69.4, 76.7 and 79.07, which were showing similarity with a JCPDS (Joint Committee on Powder Diffraction Standards) file (No. 34-0394) for pure cerium oxide. Figure 4 shows XRD pattern of Pd-Ni/AC-CeO₂ nanoparticles. Ni peaks were observed at 2 theta values of 37.5, 44 and 63, which showed an agreement with literature [37] whereas Pd presence was shown at 2θ values at 42.8 and 69.7 [38].

Figure 5 shows the EDX spectrum of Pd-Ni/AC-CeO₂, which showed the characteristic peaks of palladium, nickel, carbon, cerium and oxygen in NPs.

3.2. Effect of Adsorbent Dosage and pH

For optimization of AO-8 dye adsorption, the adsorbent dosage of Pd-Ni/AC-CeO₂ in the range 0.005–0.03 g was tested. Figure 6a shows a linear increase in removal efficiency along with an increase of adsorbent dosage up to 0.01 g of adsorbent dosage, which was attributed to the increase of adsorbent surface area and greater availability of adsorption active sites. Therefore, 0.01 g of adsorbent dosage was selected as an optimal dosage and was used for further tests.

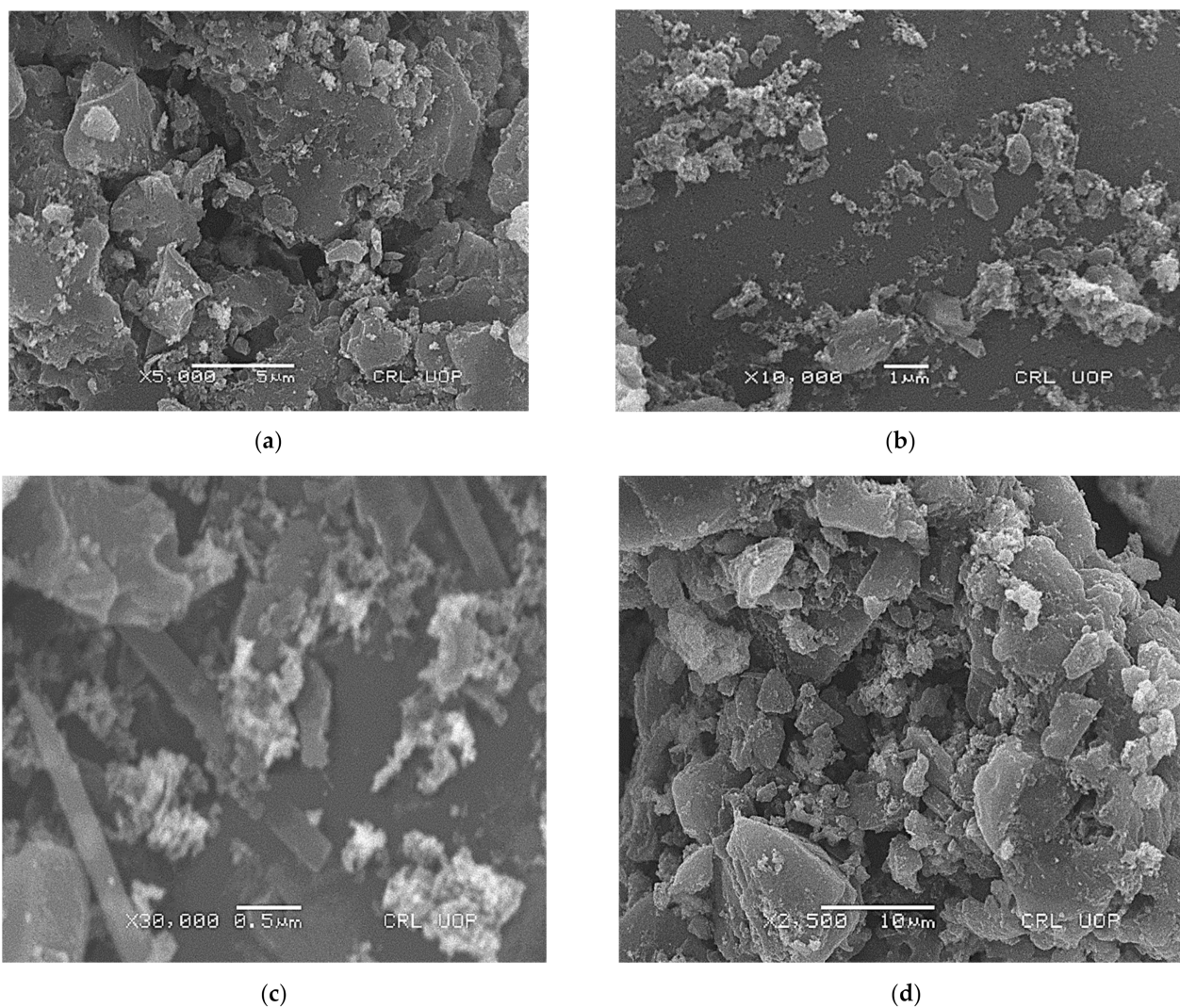


Figure 3. Scanning electron microscope (SEM) images of Pd-Ni/AC-CeO₂ on various resolutions and magnifications of: (a) 5000×, (b) 10,000×, (c) 30,000×, (d) 2500× magnification.

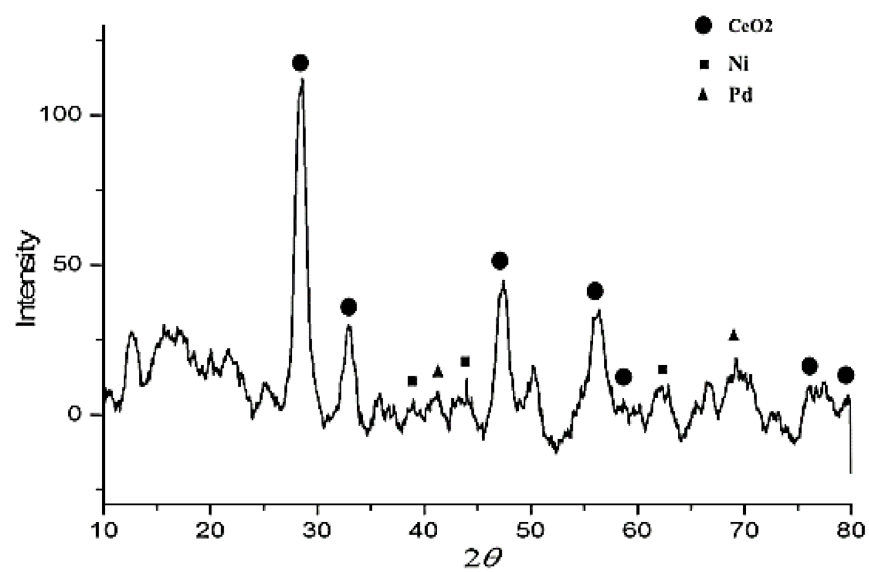


Figure 4. Powder X-ray diffraction of Pd-Ni/AC-CeO₂.

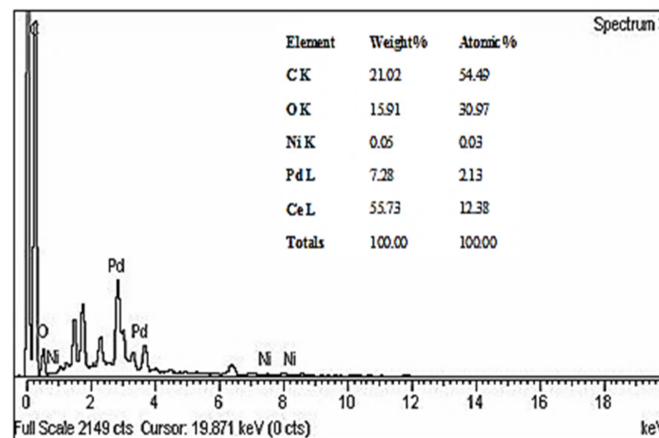


Figure 5. EDX analysis of Pd-Ni/AC-CeO₂.

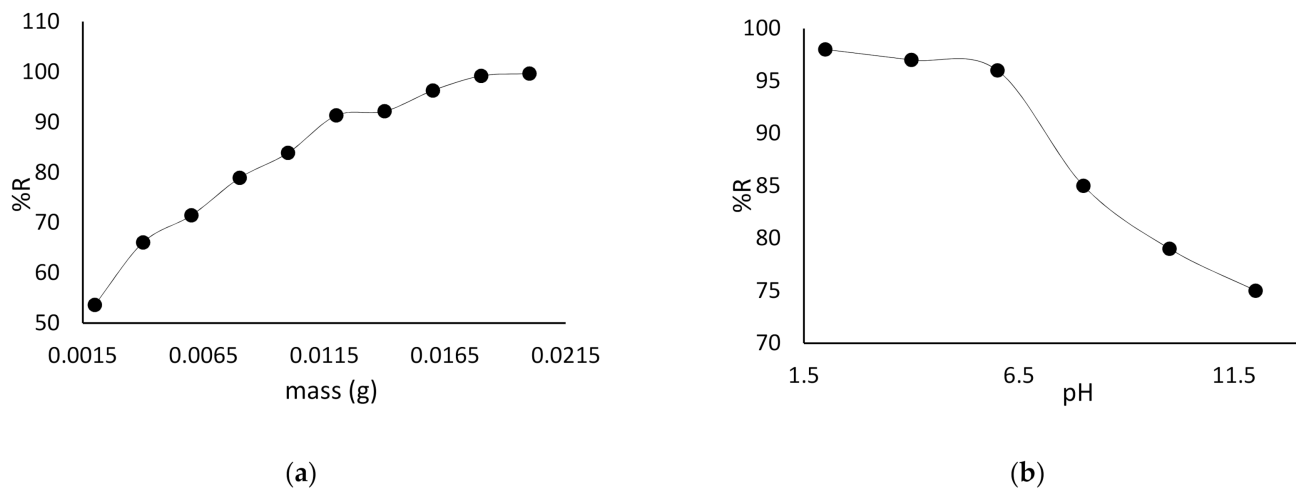


Figure 6. Effects on AO-8 removal efficiency by (a) adsorbent dosage. (b) pH.

The effect of pH on adsorption of selected dye within the tested range is given in Figure 6b showing that maximum adsorption took place from pH 2 to 5. Because of the high H⁺ ion concentration at low pH, the surface of the adsorbent was protonated and, on the other hand, dye is anionic in nature, thus an electrostatic attraction was established at low pH and a high dye removal capacity was observed. The second positive adsorption-contributing factor was the soft–soft interaction between functional groups present at adsorbate and at the metal center present at the adsorbent surface. At a low pH (2–5), electrostatic interaction between adsorbent and dye and the dye–metal center were high and resulted in a high removal efficiency of selected dye from solution. At a higher pH, decrease in removal percentage of AO-8 might be due to hydroxide ion competition with AO-8 molecules for adsorption sites on adsorbent surface [32].

3.3. Adsorption Kinetics

It is necessary to consider adsorption kinetics for precise adsorption process assessment. Adsorption kinetics are used for the determination of the adsorption mechanism, adsorbate–adsorbent interaction and adsorption characteristics. For this purpose, 0.01 g Pd-Ni/AC-CeO₂ was added to series of 10 mL flasks containing 100 mg/L AO-8 solutions. These flasks were shaken from 5 to 30 min at 293, 313, and 333 K temperature. Analysis of experimental data at different intervals made it possible to calculate the kinetic parameter, which in turn provided some information on feasibility of the process [34].

The equilibrium time of AO-8 adsorption on prepared nanoparticles is given in Figure 7 at three different temperatures. Equilibrium was reached from 5 to 6 min. Initially, the adsorption sites available were higher as a result fast adsorption occurring, which then gradually decreased to a steady state.

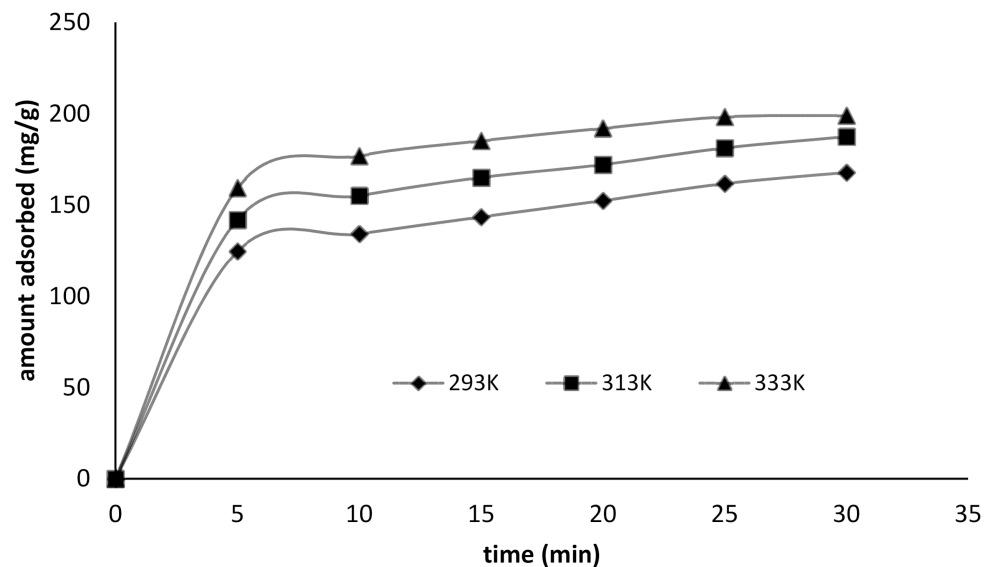


Figure 7. Adsorption kinetics for the adsorption of AO-8 Pd-Ni/AC-CeO₂.

A number of kinetics models are used to explain the kinetics of adsorption process. The different models applied in this study are given as follows:

Pseudo-first order equation [39]:

$$\log(q_e - q_t) = \log(q_e) - \frac{k_1}{2.303}t \quad (3)$$

Second-order Lagergren equation [39]:

$$\left(\frac{t}{q_e}\right) = \frac{1}{k_2 q_e^2} + \frac{1}{q_e}t \quad (4)$$

Elovich equation [39]:

$$q_t = \ln \frac{\beta \alpha}{\alpha} + \frac{\ln t}{\beta} \quad (5)$$

Intra-particle diffusion model [39]:

$$q_t = k_{id}t^{\frac{1}{2}} + C \quad (6)$$

In these equations: q_e and q_t are the adsorption capacities at equilibrium and time (t), respectively (mg/g), k_1 is the rate constant of pseudo-first order adsorption (1/min), k_2 is the rate constant of pseudo-second order adsorption (g/mg/min), α is the initial adsorption rate (mg/g min) and β is the desorption constant (mg/g min, C is the intercept and k_{id} is the intra-particle diffusion constant (mg/g min^{1/2}) [39].

The experimental results were applied to the different models, which are shown in (Figure 8a–d). From the data it is clear that the linear correlation coefficients for the pseudo-first order model were lower as compared to the pseudo-second order model and a very large difference existed between experimental and calculated q_e for the pseudo-first order model as well showing the inapplicability of this model to describe the kinetic of the adsorption process. Thus, the pseudo-second order model was found to be the best model

that can better fit the kinetic data rather than the pseudo-first order model, which confirms the chemical nature of the sorption process [40,41].

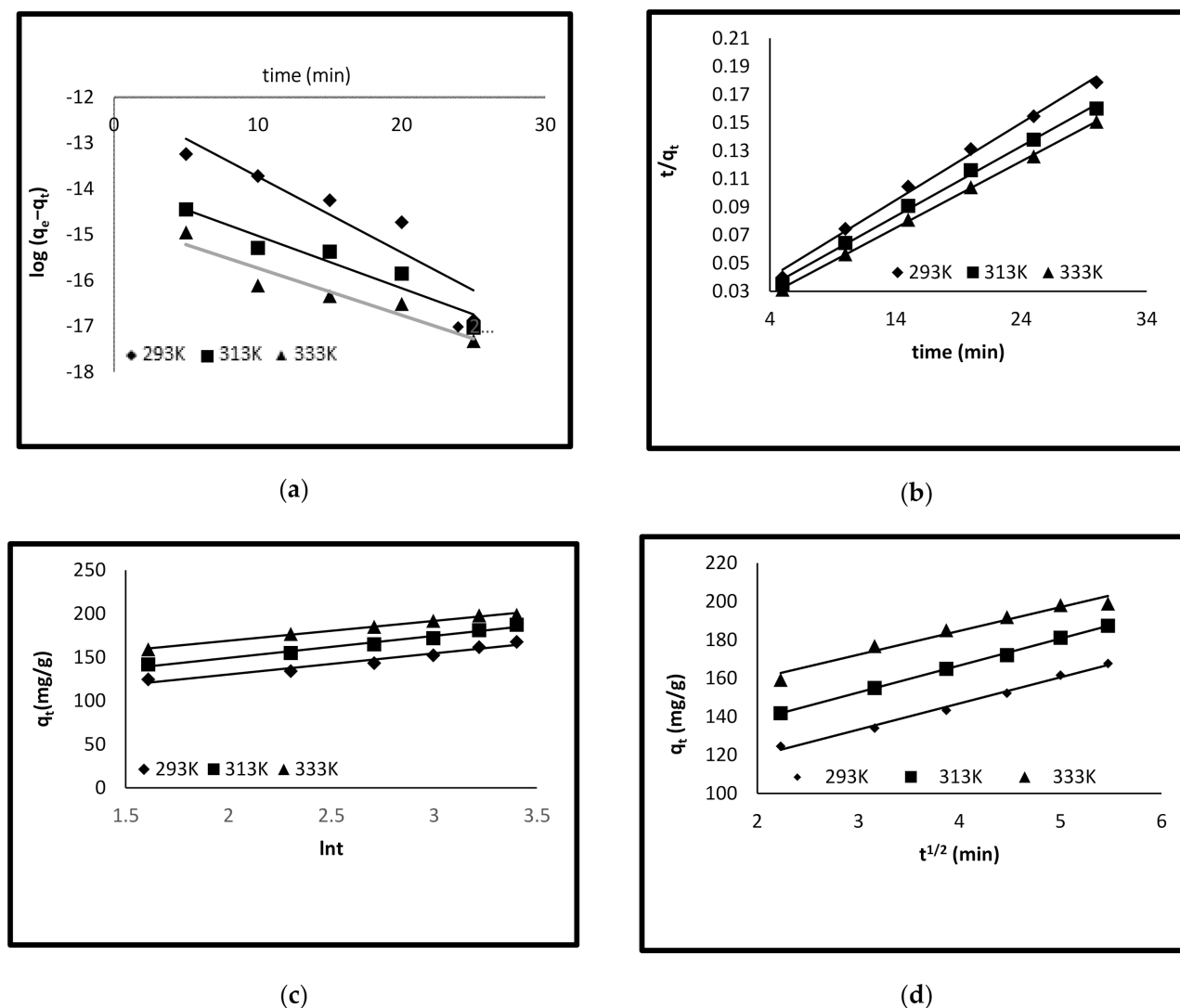


Figure 8. Kinetic models for adsorption of AO-8 on Pd-Ni/AC-CeO₂. (a) Pseudo 1st order kinetics. (b) Pseudo 2nd order kinetics. (c) Elovich model. (d) Intra particle diffusion model.

The Elovich model (Figure 8c) was also applied for adsorption of dye on prepared adsorbent at different temperature [42]. The values of different parameters of this model are given in Table 2.

The intraparticle diffusion plot (Figure 8d) between $t^{1/2}$ and q_t shows multilinearity for the adsorption of AO-8 onto Pd-Ni/AC-CeO₂ indicating that the processes under study involves more than one kinetic step. Various diffusion steps involved are explained as follows.

The first step is the fastest step that can be attributed the diffusion of AO-8 from solution towards the adsorbent surface. The second step is a slow step that corresponds to the intraparticle diffusion where adsorption increases with an increase in temperature. The third step is the diffusion through the small pores followed by an establishment of equilibrium [41]. The parameters calculated for this model are given in Table 2.

3.4. Isotherm Study

To determine the surface properties and affinity of the adsorbent, various isotherm models were used. The isotherm study was also important for the description of how the adsorbate interacts with adsorbent and gives data about adsorption capacities. The surface of the adsorbent could be occupied by adsorbate with the formation of monolayer or multilayer. To determine different isotherm parameters, Langmuir, Freundlich and Temkin models were used [43,44].

Table 2. Parameters table for different kinetic models for adsorption of AO-8 on Pd-Ni/AC-CeO₂.

Parameters	293 K	313 K	333 K
q _e (mol/g)	167.764	187.3706	198.9441
%R	83.87	93.68	99.47
Pseudo-first order			
q _e (cal) (mg/g)	82.22	82.451	99.174
k ₁ (min ⁻¹)	-0.0937	-0.0946	-0.1473
R ²	0.9264	0.949	0.9478
Pseudo-second order			
q _e (cal) (mg/g)	181.81	200	212
k ₂ (g/mg/min)	0.0016	0.00181	0.00252
R ²	0.9942	0.9967	0.9996
Elovich equation			
α (mg/g min)	691.83	1270.6	5152.3
β (mg/g min)	0.041	0.0397	0.044
R ²	0.9534	0.980	0.9933
Intra-particle diffusion			
k _{id} (mg/g min ^{-1/2})	13.623	14.022	12.364
C	92.362	110.5	135.16
R ²	0.9918	0.9988	0.9634

3.4.1. Langmuir Isotherm

In order to explain the sorption of selected dye on the prepared adsorbent, the Langmuir model was used. This model defines that the sorption process takes place at specific homogenous sites of the adsorbent and it only forms a monolayer on the surface. The linear form of this model can be given as follows:

$$\frac{C_e}{q_e} = \frac{C_e}{Q_m} + \frac{1}{K_L Q_m} \quad (7)$$

where q_e, C_e, K_L and Q_m are the adsorbed amount of dye adsorbed at equilibrium (mg/g), concentration of dye solution at equilibrium (mg/L), Langmuir constant (L/g) and the maximum adsorption capacity (mg/g), respectively [45]. A plot C_e/q_e versus C_e (from slope and intercept) enabled us to define the K_L and Q_m values (Figure 9) and their values along with the correlation coefficient R² are given in Table 2. The Langmuir adsorption maximum capacities were found to be 666, 714, and 769 mg/g at 293, 313 and 333 K, respectively. The Langmuir isotherm showed the best correlation coefficient R² value and, therefore, correlated best with tests.

3.4.2. Freundlich Isotherm Model

This model describes behavior of non-ideal and reversibility of adsorption being non-restricted to the monolayer formation. This model can be applied to adsorption on heterogeneous surfaces (multilayer adsorption) and non-uniform distribution of adsorption heat and affinities of the sites over the adsorbent surface. This model was shown as:

$$\ln q_e = \ln K_f + \frac{1}{n} \ln C_e \quad (8)$$

q_e , C_e , K_f , and $1/n$ representing the quantity of adsorbate at equilibrium, equilibrium concentration of dye solution, adsorption capacity at unit concentration and adsorption intensity.

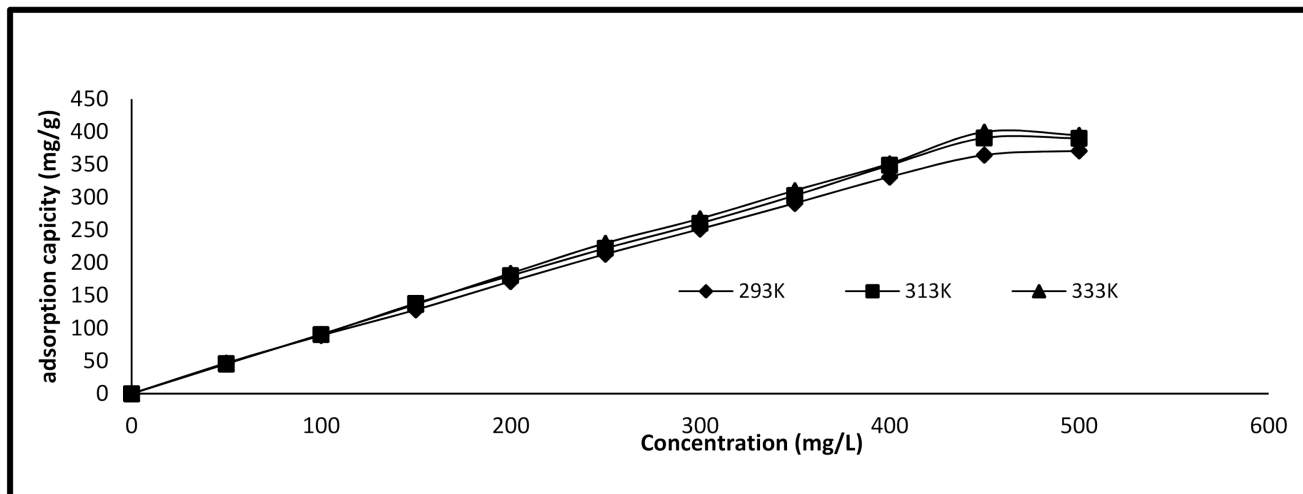


Figure 9. Absorption isotherm equilibrium for adsorption of AO-8 on Pd-Ni/AC-CeO₂.

It should be noted that when ($1/n = 0$) the type of isotherm will be irreversible and when ($0 < 1/n < 1$) will be favorable and ($1/n > 1$) will be unfavorable [46].

A plot of $\ln q_e$ versus C_e makes it possible to the quantities of n and K_f from the slope and gives the intercept (Figure 10d–f). The values of these parameters are given in Table 3. The values of $1/n$ were found to be 0.6425, 0.7435 and 0.8136 at 293, 313 and 333 K, respectively, which indicate the favorability of the adsorption process.

Table 3. Different isotherm parameters for adsorption of AO-8 on Pd-Ni/AC-CeO₂.

Parameter	293 K	313 K	333 K
Langmuir isotherm model			
Q_m (mg/g)	666.6	714	769
K_a (g/mg)	0.0136	0.0174	0.01763
R^2	0.9161	0.9262	0.9269
R_L	0.128	0.103	0.101
Freundlich isotherm model			
$1/n$	0.6425	0.7435	0.8136
K_f	20.46	18.03	15.81
R^2	0.891	0.9125	0.891
Temkin isotherm model			
B_1	107.7	126.05	139.59
K_T	0.261	0.265	0.255
R^2	0.8631	0.9391	0.9686

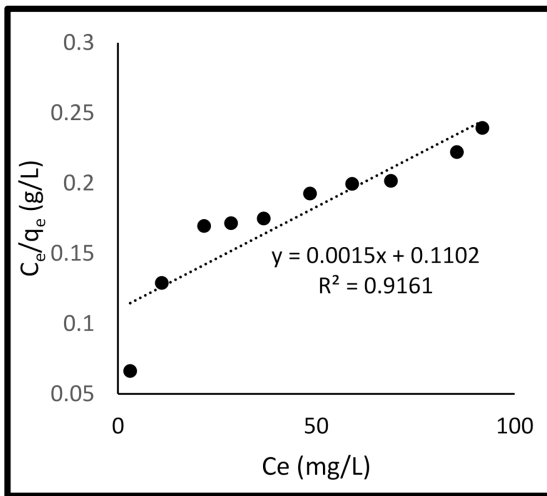
3.4.3. Temkin Isotherm Model

In the linear form this isotherm can be given as follows:

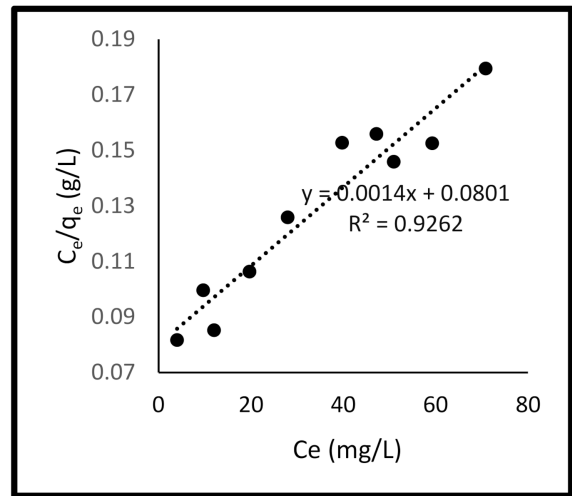
$$q_e = B_1 \ln K_T + B_1 \ln C_e \tag{9}$$

where: B_1 and K_T are constants of adsorption and equilibrium binding (L/mg), respectively [47]. A dependence q_e versus $\ln C_e$ gives us constants based on the values of these (Figure 10g–i) and respective values are shown in Table 3.

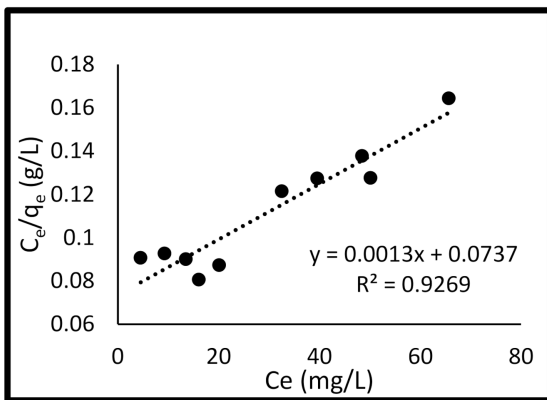
According to Table 3, the regression values are higher for the Langmuir isotherm rather than Freundlich and Temkin models.



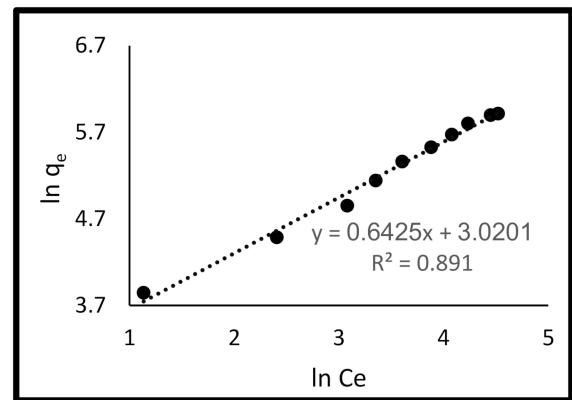
(a)



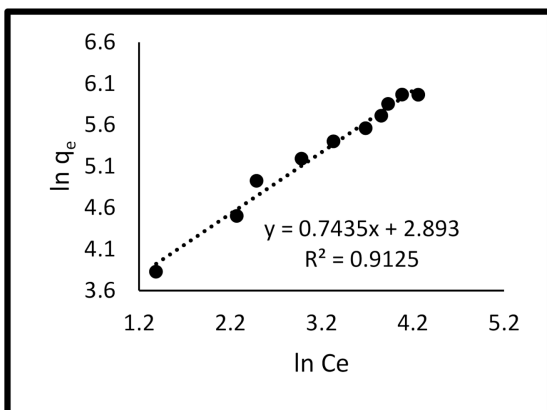
(b)



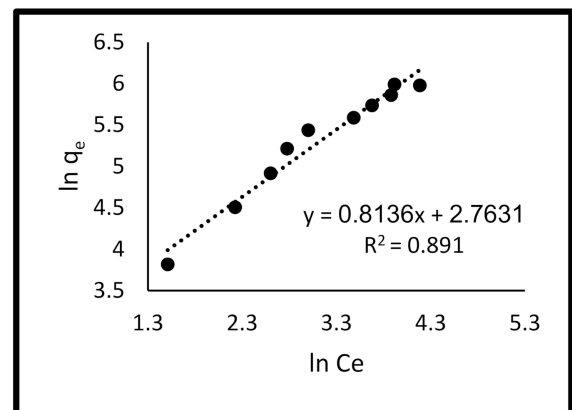
(c)



(d)



(e)



(f)

Figure 10. Cont.

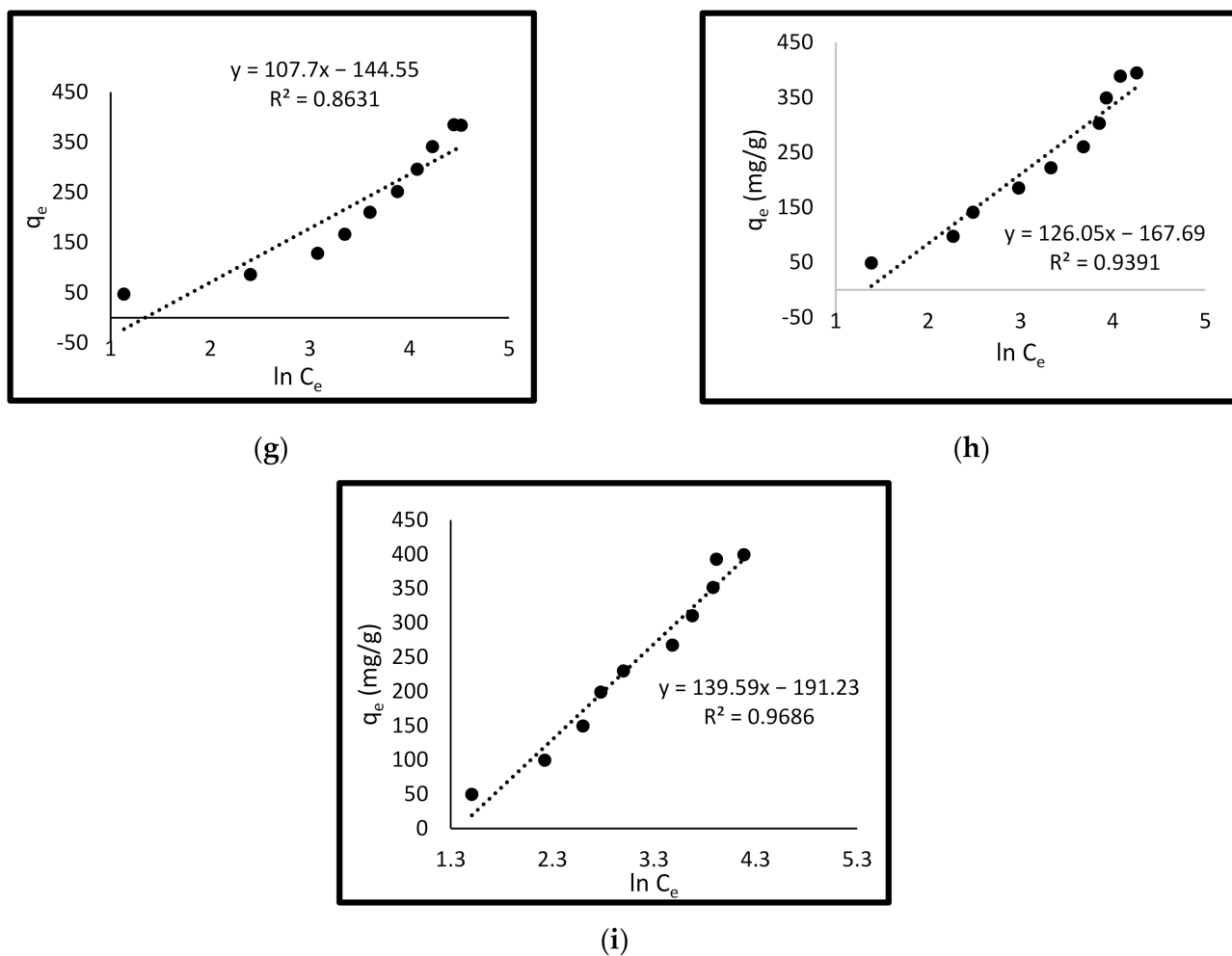


Figure 10. Adsorption isotherm models. (a) Langmuir isotherm at 293 K. (b) Langmuir isotherm. (c) Langmuir isotherm. (d) Freundlich isotherm. (e) Freundlich isotherm. (f) Freundlich isotherm. (g) Temkin isotherm. (h) Temkin isotherm. (i) Temkin isotherm.

3.5. Thermodynamic Study

The thermodynamic parameters for the adsorption of AO-8 performance on the Pd-Ni/AC-CeO₂ nanoparticles were calculated using following equations:

$$\Delta G^\circ = -RT \ln K_d \tag{10}$$

where $K_d = \frac{q_e}{C_e}$

$$\ln(K_d) = \frac{\Delta S^\circ}{R} - \frac{\Delta H^\circ}{RT} \tag{11}$$

In these equations ΔG° , ΔH° and ΔS° are the differences in Gibbs free energy, enthalpy and entropy, respectively. A dependence $\ln K_d$ versus $1/T$ defines the parameters of ΔH° and ΔS° that are usually obtained from the slope and intercept of the resultant plot. Their values are given in Table 4.

Table 4. Thermodynamic parameters for adsorption of AO-8 on Pd-Ni/AC-CeO₂.

	ΔG° kJ/mol			ΔH° kJ/mol	ΔS° kJ/ molK
	293 K	313 K	333 K		
	-18.7327	-19.4870	-20.584	-7.593	0.0384

The values of Gibbs free energy (ΔG°) were negative at all temperatures indicating the feasibility of the adsorption process and its spontaneous nature. The observed decrease in ΔG° values with increase in temperature suggests that the higher temperature would facilitate the adsorption process [48]. The negative value of ΔH° indicates the exothermic nature of the process and the positive value of entropy shows the increase in randomness at the dye/adsorbent interfaces and the feasibility of the process [49]. Previous researches have been performed assessing the effect of pH and other factors on the material performance, which could be done similarly in future studies [50–52].

3.6. Regeneration of Pd-Ni/AC-CeO₂

In order to determine the reusability of the Pd-Ni/AC-CeO₂ adsorbent, the nanoparticles were used several times and the removal efficiency was monitored. It is evident from Figure 11 that the removal efficiency was reduced to 80% after 6 cycles.

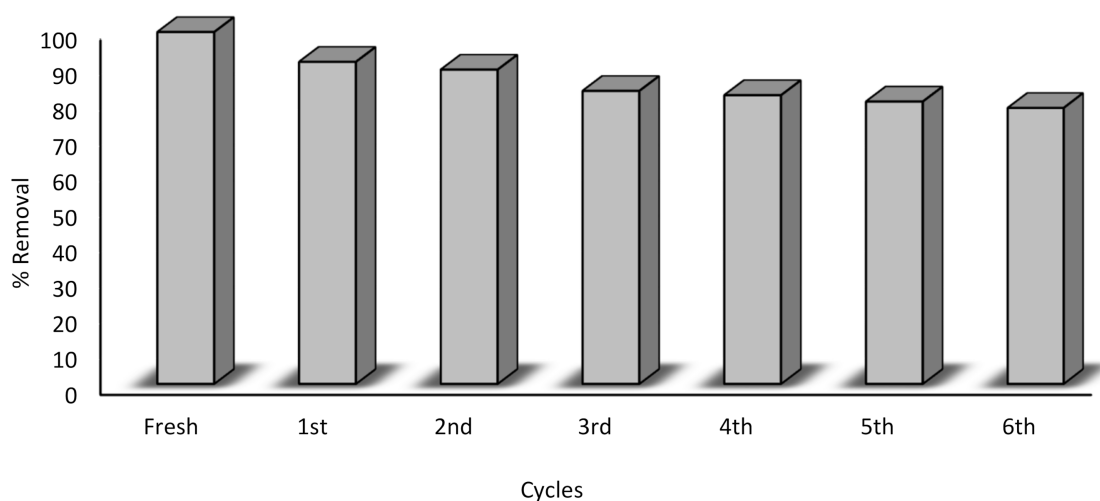


Figure 11. Regeneration of adsorbent and its percentage removal per cycle.

4. Conclusions

In this study, palladium-nickel (Pd-Ni) nanoparticles supported on activated carbon and cerium oxide were prepared and characterized through various instrumental techniques. The particles acted as an efficient adsorbent for the removal of acid orange 8 with more than 90% removal efficiency. The XRD and SEM data concluded the presence of alloy formation between Pd and Ni. The carbon and cerium oxide-based composites were used as adsorbents for the effective removal of AO-8. Different kinetics and equilibrium models were applied to calculate the adsorption parameters. Langmuir and pseudo-second order kinetics models explained the adsorption data well while the thermodynamic aspects of the adsorption process were exothermic, spontaneous and favorable with an increase in temperature. The prepared adsorbent could effectively be used to remove dyes and other pollutants from water. However, further studies are needed to completely evaluate the applicability and effectiveness of this novel bimetallic adsorbent in the case of it being used as an adsorbent for other dyes' and pollutants' removal from water.

Author Contributions: Conceptualization, M.Z.; methodology, A.U.; software, A.U.; validation, S.S.d.R., A.U. and I.Z.; formal analysis, A.U., J.B., A.K. and N.P.; investigation, A.U.; resources, M.Z.; data curation, S.A.; writing—original draft preparation, I.Z.; writing—review and editing, M.S.K. and M.Z. visualization, M.S.K.; G.D.B.; supervision, M.Z.; project administration, M.Z.; funding acquisition, M.Z. All authors have read and agreed to the published version of the manuscript.

Funding: This research was funded by project nr T190087MIMV and European Commission, MLTKT19481R “Identifying best available technologies for decentralized wastewater treatment and resource recovery for India, SLTKT20427” Sewage sludge treatment from heavy metals, emerg-

ing pollutants and recovery of metals by fungi and by project KIK 15392 and 15401 by European Commission.

Institutional Review Board Statement: Not applicable.

Informed Consent Statement: Not applicable.

Data Availability Statement: The data presented in this study is available on request from the corresponding author.

Acknowledgments: The authors are thankful to HEC, Pakistan and CRL, Peshawar Pakistan for helping in instrumental analysis.

Conflicts of Interest: The authors declare no conflict of interest. The funders had no role in the design of the study; in the collection, analyses, or interpretation of data; in the writing of the manuscript; or in the decision to publish the results.

References

- Ikram, M.; Zahoor, M.; Batiha, G.E.-S. Biodegradation and decolorization of textile dyes by bacterial strains: A biological approach for wastewater treatment. *Z. Phys. Chem.* **2020**. [[CrossRef](#)]
- Khayam, S.M.U.; Zahoor, M.; Khan, E.; Shah, M. Reduction of keto group in drimarene blue by *Aspergillus niger*; a predominant reason for subsequent decolorization. *Fresenius Environ. Bull.* **2020**, *29*, 1397–1410.
- Ikram, M.; Zahoor, M.; Khan, E.; Khayam, S.M.U. Biodegradation of Novacron Turqueiose (Reactive Blue 21) by *Pseudomonas aeruginosa*. *J. Chem. Soc. Pak.* **2020**, *42*, 737–745.
- Sarkar, S.; Banerjee, A.; Halder, U.; Biswas, R.; Bandopadhyay, R. Degradation of Synthetic Azo Dyes of Textile Industry: A Sustainable Approach Using Microbial Enzymes. *Water Conserv. Sci. Eng.* **2017**, *2*, 121–131. [[CrossRef](#)]
- Wilson, M.; Kannangara, K.; Smith, G.; Simmons, M.; Raguse, B. *Nanotechnology: Basic Science and Emerging Technologies*; Chapman and Hall/CRC: London, UK, 2002.
- Kolhatkar, A.G.; Jamison, A.C.; Litvinov, D.; Willson, R.C.; Lee, T.R. Tuning the Magnetic Properties of Nanoparticles. *Int. J. Mol. Sci.* **2013**, *14*, 15977–16009. [[CrossRef](#)] [[PubMed](#)]
- Guo, D.; Xie, G.; Luo, J. Mechanical properties of nanoparticles: Basics and applications. *J. Phys. D Appl. Phys.* **2014**, *47*, 013001. [[CrossRef](#)]
- Sosa, I.O.; Noguez, C.; Barrera, R.G. Optical Properties of Metal Nanoparticles with Arbitrary Shapes. *J. Phys. Chem. B* **2003**, *107*, 6269–6275. [[CrossRef](#)]
- Schmid, G.; Simon, U. Gold nanoparticles: Assembly and electrical properties in 1–3 dimensions. *Chem. Commun.* **2005**, *6*, 697–710. [[CrossRef](#)]
- Delannoy, L.; El Hassan, N.; Musi, A.; Le To, N.N.; Krafft, J.-M.; Louis, C. Preparation of Supported Gold Nanoparticles by a Modified Incipient Wetness Impregnation Method. *J. Phys. Chem. B* **2006**, *110*, 22471–22478. [[CrossRef](#)]
- Yang, Y.; Cui, J.; Zheng, M.; Hu, C.; Tan, S.; Xiao, Y.; Yang, Q.; Liu, Y. One-step synthesis of amino-functionalized fluorescent carbon nanoparticles by hydrothermal carbonization of chi-tosan. *Chem. Commun.* **2012**, *48*, 380–382. [[CrossRef](#)]
- Makovec, D.; Košak, A.; Žnidaršič, A.; Drogenik, M. The synthesis of spinel-ferrite nanoparticles using precipitation in microemulsions for ferrofluid applications. *J. Magn. Mater.* **2005**, *289*, 32–35. [[CrossRef](#)]
- Chen, Q.; Rondinone, A.J.; Chakoumakos, B.C.; Zhang, Z.J. Synthesis of superparamagnetic MgFe₂O₄ nanoparticles by coprecipitation. *J. Magn. Mater.* **1999**, *194*, 1–7. [[CrossRef](#)]
- Acsente, T.; Negrea, R.F.; Nistor, L.C.; Logofatu, C.; Matei, E.; Birjega, R.; Grisolia, C.; Dinescu, G. Synthesis of flower-like tungsten nanoparticles by magnetron sputtering combined with gas aggregation. *Eur. Phys. J. D* **2015**, *69*, 161. [[CrossRef](#)]
- Swihart, M.T. Vapor-phase synthesis of nanoparticles. *Curr. Opin. Colloid Interface Sci.* **2003**, *8*, 127–133. [[CrossRef](#)]
- Sanvicens, N.; Marco, M.P. Multifunctional nanoparticles—properties and prospects for their use in human medicine. *Trends Biotechnol.* **2008**, *26*, 425–433. [[CrossRef](#)] [[PubMed](#)]
- Kokura, S.; Handa, O.; Takagi, T.; Ishikawa, T.; Naito, Y.; Yoshikawa, T. Silver nanoparticles as a safe preservative for use in cosmetics. *Nanomed. Nanotechnol. Biol. Med.* **2010**, *6*, 570–574. [[CrossRef](#)]
- Wei, Q. *Surface Modification of Textiles*; Elsevier: Amsterdam, The Netherlands, 2009.
- Nawaz, H.R.; Solangi, B.A.; Zehra, B.; Nadeem, U. Preparation of nano zinc oxide and its application in leather as a retanning and antibacterial agent. *Can. J. Sci. Ind. Res.* **2011**, *2*, 164–170.
- Ogolo, N.A.; Olafuyi, O.A.; Onyekonwu, M.O. Enhanced Oil Recovery Using Nanoparticles. In Proceedings of the SPE Saudi Arabia Section Technical Symposium and Exhibition, Al-Khobar, Saudi Arabia, 8–11 April 2012. [[CrossRef](#)]
- Xia, Y.; Yang, H.; Campbell, C.T. Nanoparticles for Catalysis. *Acc. Chem. Res.* **2013**, *46*, 1671–1672. [[CrossRef](#)]
- Sankar, R.; Manikandan, P.; Malarvizhi, V.; Fathima, T.; Shivashangari, K.S.; Ravikumar, V. Green synthesis of colloidal copper oxide nanoparticles using *Carica papaya* and its application in photocatalytic dye degradation. *Spectrochim. Acta Part A Mol. Biomol. Spectrosc.* **2014**, *121*, 746–750. [[CrossRef](#)]

23. Mak, S.-Y.; Chen, D.-H. Fast adsorption of methylene blue on polyacrylic acid-bound iron oxide magnetic nanoparticles. *Dye. Pigment.* **2004**, *61*, 93–98. [[CrossRef](#)]
24. Saifuddin, N.; Nian, C.; Zhan, L.; Ning, K. Chitosan-silver Nanoparticles Composite as Point-of-use Drinking Water Filtration System for Household to Remove Pesticides in Water. *Asian J. Biochem.* **2011**, *6*, 142–159. [[CrossRef](#)]
25. Couvreur, P.; Kante, B.; Roland, M.; Speiser, P. Adsorption of Antineoplastic Drugs to Polyalkylcyanoacrylate Nanoparticles and Their Release in Calf Serum. *J. Pharm. Sci.* **1979**, *68*, 1521–1524. [[CrossRef](#)]
26. Rahmani, A.; Mousavi, H.Z.; Fazli, M. Effect of nanostructure alumina on adsorption of heavy metals. *Desalination* **2010**, *253*, 94–100. [[CrossRef](#)]
27. Gautam, R.K.; Rawat, V.; Banerjee, S.; Sanroman, M.A.; Soni, S.; Singh, S.K.; Chattopadhyaya, M.C. Synthesis of bimetallic Fe–Zn nanoparticles and its application towards adsorptive removal of carcinogenic dye malachite green and Congo red in water. *J. Mol. Liq.* **2015**, *212*, 227–236. [[CrossRef](#)]
28. Duran, C.; Ozdes, D.; Gundogdu, A.; Senturk, H.B. Kinetics and Isotherm Analysis of Basic Dyes Adsorption onto Almond Shell (*Prunus dulcis*) as a Low Cost Adsorbent. *J. Chem. Eng. Data* **2011**, *56*, 2136–2147. [[CrossRef](#)]
29. Chen, K.-C.; Wu, J.-Y.; Huang, C.-C.; Liang, Y.-M.; Hwang, S.-C.J. Decolorization of azo dye using PVA-immobilized microorganisms. *J. Biotechnol.* **2003**, *101*, 241–252. [[CrossRef](#)]
30. Bhattacharya, A.; Naiya, T.; Mandal, S.; Das, S. Adsorption, kinetics and equilibrium studies on removal of Cr(VI) from aqueous solutions using different low-cost adsorbents. *Chem. Eng. J.* **2008**, *137*, 529–541. [[CrossRef](#)]
31. Belhachemi, M.; Addoun, F. Comparative adsorption isotherms and modeling of methylene blue onto activated carbons. *Appl. Water Sci.* **2011**, *1*, 111–117. [[CrossRef](#)]
32. Ghaedi, M.; Heidarpour, S.; Kokhdan, S.N.; Sahraie, R.; Daneshfar, A.; Brazesh, B. Comparison of silver and palladium nanoparticles loaded on activated carbon for efficient removal of Methylene blue: Kinetic and isotherm study of removal process. *Powder Technol.* **2012**, *228*, 18–25. [[CrossRef](#)]
33. Asfaram, A.; Ghaedi, M.; Hajati, S.; Rezaeinejad, M.; Goudarzi, A.; Purkait, M.K. Rapid removal of Auramine-O and Methylene blue by ZnS: Cu nanoparticles loaded on activated carbon: A re-sponse surface methodology approach. *J. Taiwan Inst. Chem. Eng.* **2015**, *53*, 80–91. [[CrossRef](#)]
34. Roosta, M.; Ghaedi, M.; Shokri, N.; Daneshfar, A.; Sahraei, R.; Asghari, A. Optimization of the combined ultrasonic assisted/adsorption method for the removal of malachite green by gold nanoparticles loaded on activated carbon: Experimental design. *Spectrochim. Acta Part A Mol. Biomol. Spectrosc.* **2014**, *118*, 55–65. [[CrossRef](#)] [[PubMed](#)]
35. Zhu, H.; Jia, Y.; Wu, X.; Wang, H. Removal of arsenic from water by supported nano zero-valent iron on activated carbon. *J. Hazard. Mater.* **2009**, *172*, 1591–1596. [[CrossRef](#)]
36. Arabzadeh, S.; Ghaedi, M.; Ansari, A.; Taghizadeh, F.; Rajabi, M. Comparison of nickel oxide and palladium nanoparticle loaded on activated carbon for efficient removal of methylene blue: Kinetic and isotherm studies of removal process. *Human Exp. Toxicol.* **2015**, *34*, 153–169. [[CrossRef](#)] [[PubMed](#)]
37. da Silva, A.; Bion, N.; Epron, F.; Baraka, S.; Fonseca, F.; Rabelo-Neto, R.; Mattos, L.; Noronha, F. Effect of the type of ceria dopant on the performance of Ni/CeO₂ SOFC anode for ethanol internal reforming. *Appl. Catal. B Environ.* **2017**, *206*, 626–641. [[CrossRef](#)]
38. Chrzan, M.; Chlebda, D.; Jodłowski, P.; Salomon, E.; Kołodziej, A.; Gancarczyk, A.; Sitarz, M.; Łojewska, J. Towards methane combustion mechanism on metal oxides supported catalysts: Ceria supported palladium catalysts. *Top. Catal.* **2019**, *62*, 403–412. [[CrossRef](#)]
39. Önal, Y.; Akmil-Başar, C.; Sarıcı-Özdemir, Ç. Investigation kinetics mechanisms of adsorption malachite green onto activated carbon. *J. Hazard. Mater.* **2007**, *146*, 194–203. [[CrossRef](#)]
40. Crini, G. Kinetic and equilibrium studies on the removal of cationic dyes from aqueous solution by adsorption onto a cyclodextrin polymer. *Dye. Pigment.* **2008**, *77*, 415–426. [[CrossRef](#)]
41. Cheung, W.; Szeto, Y.; McKay, G. Intraparticle diffusion processes during acid dye adsorption onto chitosan. *Bioresour. Technol.* **2007**, *98*, 2897–2904. [[CrossRef](#)]
42. Largette, L.; Pasquier, R. A review of the kinetics adsorption models and their application to the adsorption of lead by an activated carbon. *Chem. Eng. Res. Design* **2016**, *109*, 495–504. [[CrossRef](#)]
43. Qiu, H.; Lv, L.; Pan, B.-C.; Zhang, Q.-J.; Zhang, W.-M.; Zhang, Q.-X. Critical review in adsorption kinetic models. *J. Zhejiang Univ. A* **2009**, *10*, 716–724. [[CrossRef](#)]
44. Saxena, M.; Sharma, N.; Saxena, R. Highly efficient and rapid removal of a toxic dye: Adsorption kinetics, isotherm, and mechanism studies on functionalized multiwalled carbon nanotubes. *Surfaces Interfaces* **2020**, *21*, 100639. [[CrossRef](#)]
45. Langmuir, I. THE ADSORPTION OF GASES ON PLANE SURFACES OF GLASS, MICA AND PLATINUM. *J. Am. Chem. Soc.* **1918**, *40*, 1361–1403. [[CrossRef](#)]
46. Freundlich, H. Over the adsorption in solution. *J. Phys. Chem.* **1906**, *57*, 1100–1107.
47. Munagapati, V.S.; Kim, D.-S. Equilibrium isotherms, kinetics, and thermodynamics studies for congo red adsorption using calcium alginate beads impregnated with nano-goethite. *Ecotoxicol. Environ. Saf.* **2017**, *141*, 226–234. [[CrossRef](#)] [[PubMed](#)]
48. Namasivayam, C.; Senthilkumar, S. Recycling of industrial solid waste for the removal of mercury (II) by adsorption process. *Chemosphere* **1997**, *34*, 357–375. [[CrossRef](#)]
49. Aljeboree, A.M.; Baqir, S.J.; Alkaim, A.F. Experimental studies of Thermodynamics parameters: As a model Adsorption and Removal of Textile. *J. Phys. Conf. Ser.* **2020**, *1664*, 012099. [[CrossRef](#)]

-
50. Tenno, T.; Rikmann, E.; Zekker, I.; Tenno, T. Modelling the solubility of sparingly soluble compounds depending on their particles size. *Proc. Est. Acad. Sci.* **2018**, *67*, 300–302. [[CrossRef](#)]
 51. Zekker, I.; Tenno, T.; Selberg, A.; Uiga, K. Dissolution Modeling and Experimental Measurement of CaS-H₂O Binary System. *Chin. J. Chem.* **2011**, *29*, 2327–2336. [[CrossRef](#)]
 52. Tenno, T.; Rikmann, E.; Uiga, K.; Zekker, I.; Mashirin, A.; Tenno, T. A novel proton transfer model of the closed equilibrium system H₂O–CO₂–CaCO₃–NH_x. *Proc. Est. Acad. Sci.* **2018**, *4017*, 2. [[CrossRef](#)]